



# Waveform inversion and focal mechanisms of two weak earthquakes in Cordillera Principal (Argentina) between 35° and 35.5° S



Raquel J. Villegas A.<sup>a, b, \*</sup>, Jiri Zahradník<sup>c</sup>, Silvina Nacif<sup>a, d</sup>, Silvana Spagnotto<sup>a, e</sup>, Diego Winocur<sup>f</sup>, Maria Flavia Leiva<sup>a, d</sup>

<sup>a</sup> Consejo Nacional de Investigaciones Científicas y Técnicas, Conicet, Argentina

<sup>b</sup> Centro de Investigaciones en Ciencias de la Tierra, Universidad Nacional de Córdoba, Av. Vélez Sarsfield 1611, Córdoba, Argentina

<sup>c</sup> Charles University in Prague, Faculty of Mathematics and Physics, V Holesovickách 2 180 00 Prague, Czech Republic

<sup>d</sup> Instituto Geofísico Sismológico F. Volponi, Universidad Nacional de San Juan, Ruta 12, Km 17, Marquesado, Rivadavia, San Juan, Argentina

<sup>e</sup> Departamento de Física, Universidad Nacional de San Luis, Ejército de los Andes 950 5700, San Luis Argentina

<sup>f</sup> Laboratorio de Tectónica Andina, Instituto de Estudios Andinos (UBA-CONICET), Argentina

## ARTICLE INFO

### Article history:

Received 19 February 2015

Received in revised form

7 October 2015

Accepted 9 December 2015

Available online 12 December 2015

### Keywords:

Moment tensor

Cordillera Principal

ISOLA

CSPS code

Weak earthquakes

Andean chain

Waveform inversion

## ABSTRACT

Only few (six) focal mechanism, in CMT Catalog, have been so far known for intraplate shallow events in the Andean chain close to Chile–Argentina state border at latitudes ~35° S. We add two more mechanisms, depths and moment magnitudes by carefully analyzing full waveforms of weak events recorded by broad-band stations of the Chile Argentina Geophysical Experiment (southern profile). The moment magnitudes of both events ( $M_w = 3.6$  and  $3.7$ ) are lower than the duration magnitudes ( $M_d = 4.0$  and  $4.29$ ) reported by NEIC. The source depth, constrained by waveforms for one of the studied events ( $5.5$ – $8.5$  km) seems to be considerably shallower than the hypocenter depth located by means of arrival times (~20 km). The waveform analysis was complemented by first-motion polarities which resulted in an uncertainty assessment of the focal mechanism. Event 1 (2001-11-03) has a strike-slip mechanism with a small normal component and almost vertical nodal planes in the north-south and east-west directions. The north-south nodal plane could be related to the Calabozos faults system. Event 2 (2002-02-16) has a strike-slip mechanism with a small thrust component. The latter event (its sub-horizontal nodal plane) could be associated with the El Diablo-El Fierro fault system. Dextral strike-slip solutions are consistent with recent studies in the area.

© 2015 Elsevier Ltd. All rights reserved.

## 1. Introduction

The subduction of the Nazca plate beneath the South American plate generates the mountain building in the Andes. In these active margins large interplate underthrusting earthquakes occur and are the main goals of several research works (Christensen and Ruff, 1988; Beck et al., 1998; Moreno et al., 2009; Lange et al., 2012; Ruiz et al., 2013; Lay, 2015; among others). Intraplate shallow earthquakes from the overriding plate exhibit lower magnitudes and their occurrence is less frequent (Fig. 1). Those earthquakes are

located in the forearc (Andean chain) and in the backarc. A noticeable aspect is the important seismicity increase between ~33° and 36° S documented by NEIC-USGS International Catalog. The only solution in CMT catalog at the latitudes analyzed in this paper is  $M_w = 6.5$ , 2004-08-28. This solution is a strike-slip focal mechanism, which could be associated to the subduction obliquity of Nazca plate (Comte et al., 2008).

Focal mechanism solutions from waveform inversion techniques are generally available for earthquakes with magnitude greater than 5.0. However, in this region majority of the seismic events has magnitudes less than 5.0 (Fig. 2). Therefore, the goal of this research is the application of moment tensor determination to waveform data available for events with magnitude less than 5.0 (<http://www.iris.edu/SeisQuery/>). Every focal mechanism of these relatively weak events is important, even if they are not numerous. This study was made possible thanks to temporary network of the Chile Argentina Geophysical Experiment

\* Corresponding author. Consejo Nacional de Investigaciones Científicas y Técnicas, Conicet, Argentina.

E-mail addresses: [Vraquelj@gmail.com](mailto:Vraquelj@gmail.com) (R.J. Villegas A.), [jz@karel.troja.mff.cuni.cz](mailto:jz@karel.troja.mff.cuni.cz) (J. Zahradník), [nacif.silvina@gmail.com](mailto:nacif.silvina@gmail.com) (S. Nacif), [pampa113@gmail.com](mailto:pampa113@gmail.com) (S. Spagnotto), [diegowinocur@hotmail.com](mailto:diegowinocur@hotmail.com) (D. Winocur), [mariaflavialeiva@gmail.com](mailto:mariaflavialeiva@gmail.com) (M.F. Leiva).

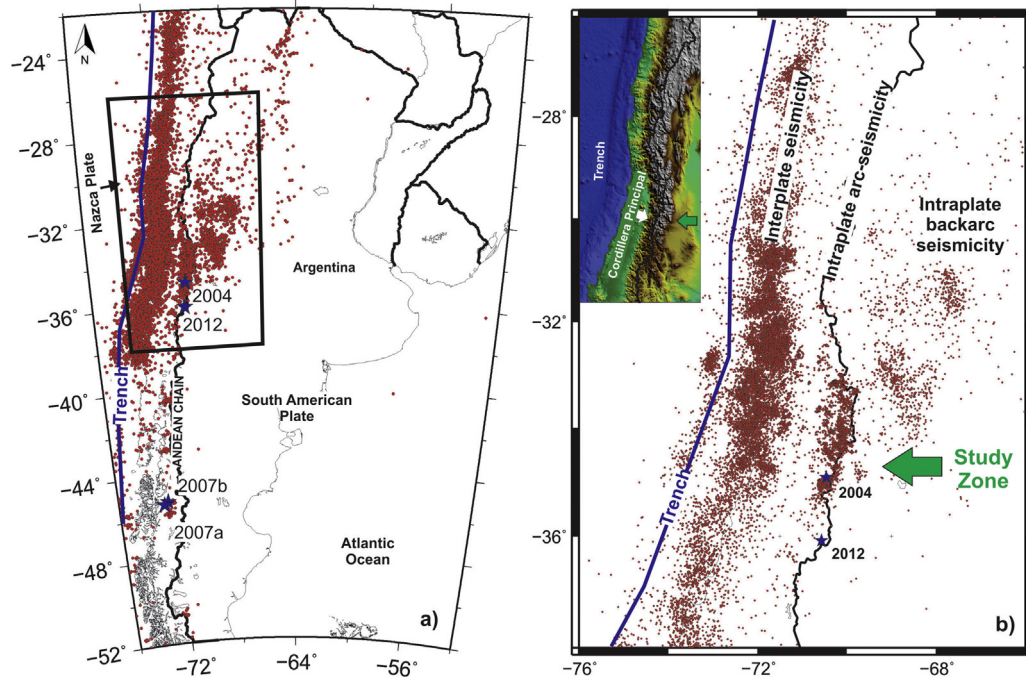


**Fig. 1.** Epicenters (red circles) from NEIC-Catalog (US Geological Survey) located between depths 0 and 50 km since January 1973 to January 2015. State borders are shown by thick black line and the Trench Zone by thick blue line; a) Blue stars denote the crustal seismicity located at the Andean chain with magnitude greater than 6.0. From north to south:  $M = 6.5$ , August 28th 2004;  $M = 6.0$ , June 6th 2012;  $M = 6.2$ , April 21st 2007 and  $M = 6.1$ , April 1st 2007 (NEIC-Catalog). There is a noticeable seismicity increase below Andean chain between  $\sim 33^\circ$  and  $36^\circ$  S. The black box shows the region plotted in b); b) The western and eastern seismicity patterns represent the interplate events related with the contact of Nazca and South American plate and intraplate events (arc and backarc seismicity) related with the overriding South America plate, respectively. Inset: Topography and bathymetry from <http://maps.ngdc.noaa.gov>; the white and green arrows indicated the "Cordillera Principal" and the study zone, respectively. (For interpretation of the references to colour in this figure legend, the reader is referred to the web version of this article.)

(CHARGE), November 2000 to May 2002. We used two methods for crustal events on the high Andes to find their centroid moment tensor solution: ISOLA software (Sokos and Zahradník, 2008, 2013) and a new approach called Cyclic Scanning of the Polarity Solution "CSPS" (Fojtíková and Zahradník, 2014). We combine the two techniques with intention to better resolve the mechanisms of the events recorded only by few stations.

## 2. Seismotectonic setting

The zone of interest corresponds to the southern Central Andes comprising the high chain of Chile and Argentina from  $35^\circ$  S to  $35.5^\circ$  S. At these latitudes, geological units and continental border strike NNE–SSW encompassing part of the southern volcanic zone. The Nazca plate is subducting underneath the South American plate with a normal angle of  $27^\circ$  (Pardo et al. 2002; Anderson et al. 2007) at a rate of  $6.7 \pm 0.2$  cm/yr, as constrained by GPS measurements along the Chile–Peru oceanic trench (Kendrick et al., 2003). As is observed in Fig. 1b, at the given latitudes the Cordillera Principal takes an important role, focusing the major seismic activity in the upper plate. Also, the higher percentage of crustal seismicity is located on the western flank of the Andean mountain chain as documented by the international catalog (NEIC-USGS or EHB-ISS), regional data (Marot, 2013) and local data (Alvarado, 1998; Barrientos et al., 2004; Nacif, 2012; Marot, 2013). This seismicity is constrained to the first 20 km of the crust (Barrientos et al., 2004). Fig. 2a and b, shows the crustal seismicity (0–50 km) for the study region and surrounding areas from NEIC Catalog (1973–2015) and the focal mechanism solutions from Harvard CMT (1976–2015) and Alvarado et al. (2009). The  $M_w = 6.5$  earthquake of August 28th 2004, located at a depth of 16 km (depth constrained from Harvard CMT) and its aftershocks sequence were recorded by a local

network in Chile. The aftershocks, located at depths less than 15 km, are distributed along a trend of the NNE–SSW direction (Comte et al., 2008), consistently with one of the nodal plane from Harvard CMT oriented NNE–SSW dextral strike-slip. In the NNE direction at  $\sim 70$  km from the 2004 earthquake a similar solution was found (Harvard CMT) for  $M_w = 5.9$ , September 13th 1987 earthquake. The actual state of the Cordillera Principal, proposed by Fariás (2007), principally presents a dextral kinematic with a forearc moving toward to the north. Also, thrust solutions are resolved by Harvard CMT. Additionally, Alvarado et al. (2009), using body-wave modeling estimated fault orientation, depth and size of  $M_w = 6.3$ , September 4th 1958, "Las Melosas" earthquake. They found a focal mechanism solution with nodal planes on an east–west and north–south direction with right–lateral and left–lateral displacement, respectively. Their interpretation focused on the activation of east–west structures, which could be accommodating differences in the higher and lower shortening to the north and south of  $\sim 33^\circ$  S respectively.

From microtectonic analysis of Quaternary faults Lavenu and Cembrano (1999), deduced the principal directions of the maximum horizontal compressional stress " $\sigma_{Hmax}$ ". They obtained a NNE–SSW direction for  $\sigma_{Hmax}$  at  $\sim 34^\circ$  S.

## 3. Data

Data are from CHile ARgentina Geophysical Experiment (CHARGE) recorded from November 2000 to May 2002. Stations were disposed in two E–W transects at  $30^\circ$  S and at  $36^\circ$  S, with other stations deployed between those transects (22 broadband stations in total). In this work only data from the southern transect were used (Fig. 3). Seismic events (magnitude  $\geq 4$ ) located at high Andes by U.S. Geological Survey (NEIC-Catalog) were selected. The

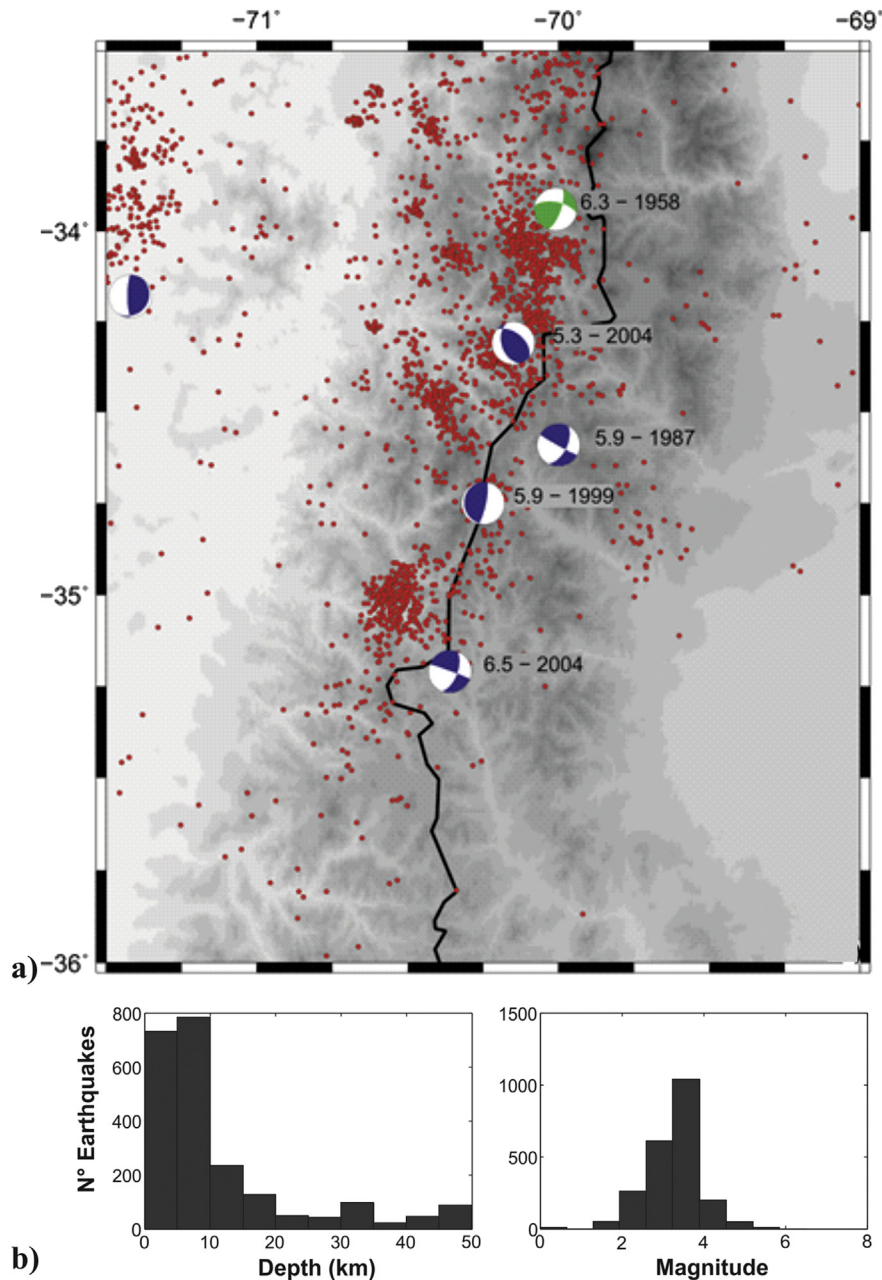


**Fig. 2.** a) The map shows the crustal seismicity for the study region for depth from 0 to 50 km. Red circles: epicenters from NEIC catalog from January 1973 to January 2015. Focal mechanism solutions from Harvard CMT Catalog (beachball in purple) and Alvarado et al. (2009; beachball in green). These are shown by lower hemisphere projections with dark colors indicating compressional quadrants. Argentina–Chile state border is shown by thick black line; b) Histograms of the focal depth and magnitude for seismic events plotted in a). Most of events have depth less than 20 km and magnitude lower than 5.0 consistently with Barrientos et al. (2004). (For interpretation of the references to colour in this figure legend, the reader is referred to the web version of this article.)

waveform data from IRIS Seismic Query ([http://www.iris.edu/SeismicQuery/breq\\_fast.phtml](http://www.iris.edu/SeismicQuery/breq_fast.phtml)) were downloaded. We relocated events using Hypocenter (Lienert and Havskov, 1995) which runs in SEISAN (Havskov et al., 2007).

#### 4. Methodology

The focal mechanism solution is one of the most important parameters of an earthquake and the focal mechanisms represent the first step to determine the stress regime of a region under study. Our goal is to calculate the focal mechanism, depth and size of 2

earthquakes of relatively small magnitudes ( $M_d$  between 4 and 4.2) in the region of interest. Two methods were used: ISOLA software (Sokos and Zahradník, 2008, 2013) and the CSPS code (Fojtíková and Zahradník, 2014).

ISOLA runs on Matlab platform allowing the users an easy interaction. ISOLA calculates the centroid moment tensor solution of an earthquake based on the least-squares inversion of full waveforms, assuming a point-source representation (multiple point sources can be studied as well, but were not used in the present paper). The program can be used for local and regional events. Green's functions are calculated by the discrete



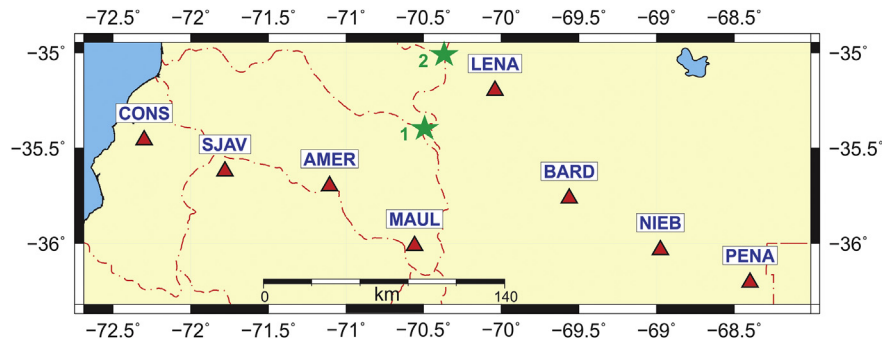


**Fig. 3.** Map with the station locations used in this work (indicated with red triangles). Those stations represent the CHARGE southern profile. Additionally, just for polarity reading, one station of the other transect of this project was also used, station LITI located at 31° S and 71° W, which is outside of this figure. The green stars (denoted 1 and 2) indicate the epicenters of two events studied in the present paper. (For interpretation of the references to colour in this figure legend, the reader is referred to the web version of this article.)

**Table 1**

Spagnotto's velocity model. The estimated depth of Mohorovicic's discontinuity is of 55 km of depth according to this model.

Depth of Layer top (km)	Vp (km/s)	Vs (km/s)
0.0	5.12	3.185
5.0	5.69	3.373
10.0	5.84	3.374
20.0	6.39	3.634
35.0	6.84	3.947
45.0	7.24	3.948
55.0	7.42	4.166
90.0	8.18	4.696
120.0	8.69	4.888
210.0	8.76	4.940

wavenumber method (Bouchon, 1981). The centroid position and centroid time are calculated by a grid search. The eigenvectors of the moment tensor provide the strike, dip and rake angles. The eigenvalues provide the scalar moment ( $M_0$ ) and decomposition of the moment tensor in three parts: double couple (DC), compensated linear vector dipole (CLVD) and isotropic or volumetric component (VOL). Their relative size is expressed in percentages; in this paper we focus on the double-couple percentage, denoted DC%. Optionally, a deviator inversion can be calculated ( $VOL = 0$ ); just this is the case of all ISOLA applications in the present paper. The low- and high-frequency limit of the waveform inversion are determined by the noise (either natural or instrumental) and by a given epicentral distance and quality of the velocity model, respectively (Fojtíková and Zahradník, 2014). The best solution is the one having the least residual error, which is equivalent to maximizing the correlation between the observed and synthetic seismograms; their match is measured by variance reduction (VR), which should be as close to 1 as possible. Resolvability of the moment tensor is quantified by the condition number (CN), which is the ratio between the maximum and minimum singular value of the Green's function matrix (Zahradník and Custodio, 2012). It is a relative measure, the smaller and larger CN values corresponding to well-posed and ill-posed inverse problems, respectively. The methodical details are described in Krizova et al. (2013).

For events recorded at only few stations some additional

constraints are needed, for example the first-motion polarities. This is the idea of the CSPS method (Fojtíková and Zahradník, 2014). To apply the CSPS code a set of polarity solutions must be provided, e.g. using code FOCMEC (Snok, 2003). The strike/dip/rake triplet from each FOCMEC solution is then used as input for the waveform inversion in which scalar moment, source position and centroid time are calculated. Every solution is quantified by variance reduction (VR) and a subset of admissible solutions is determined. To define the admissible CSPS solutions, a range close to the optimal solution is chosen, for example, the interval between 0.95 VRopt and VRopt, where VRopt denotes the best fitting solution. The advantage of CSPS is not only in using both waveforms and polarities, but also in explaining data with 100% DC source model.

Recently, the CSPS method has been also implemented in ISOLA software (unpublished modification by E. Sokos), but, for simplicity, hereafter we speak about ISOLA and CSPS as about two independent codes.

## 5. Results

The velocity model of Spagnotto (2013; see Table 1) was used for the calculation of the location and focal mechanisms, both with FOCMEC and ISOLA. The selected earthquakes with their location parameters obtained in this work using HYPOCENTER and their NEIC magnitude are shown in Table 2.

Earthquakes occurring in the period of duration of the CHARGE project and near the CHARGE stations were sought. From this set, earthquakes of magnitude  $M_d$  (NEIC) greater than 4 were selected due to the geometry of the network of stations and the noise observed in the records.

### 5.1. Event 1

This event occurred on 3rd November 2001; see more details in Table 2.

#### 5.1.1. Inversion with ISOLA

We inverted full waveforms at 5 stations (MAUL, BARD, SJAV, NIEB, PENA) using ISOLA without any prior first-motion polarity constraint, see Fig. 4. The frequency range was 0.05–0.08 Hz, and

**Table 2**

Events selected for processing.

Event	Date	Origin time (GMT)	Latitude	Longitude	Depth (km)	Latitude error (km)	Longitude error (km)	Depth error (km)	Magnitude ( $M_d$ )
1	2001 - 11 - 03	16: 30: 8.2	−35.371°	−70.526°	21.0	2.9	1.7	3.1	4.0
2	2002 - 02 - 16	06: 33: 8.8	−35.059°	−70.430°	18.1	2.0	0.8	1.6	4.2

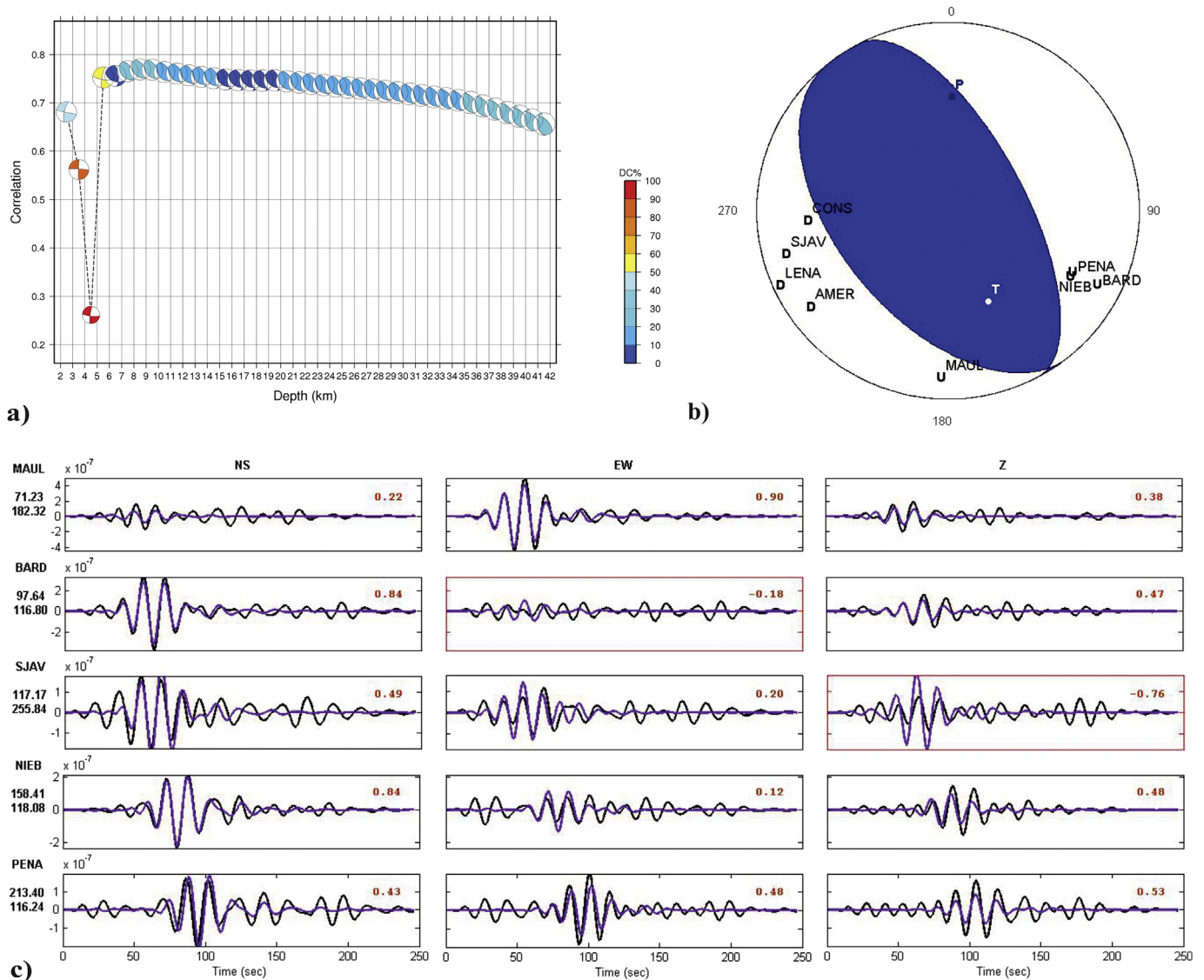


**Fig. 4.** Event 1 a) Correlation diagram demonstrating variation of the focal mechanism with the trial source depth. The optimal solution is at the depth of 8.5 km; b) The beachball representing the optimal solution calculated by ISOLA, compared with the observed first-motion polarities for the 8.5 km depth; c) Observed (black) and synthetic (purple) waveforms in the frequency range between 0.05 and 0.08 Hz. Shown in the plot are displacements (in meters). The number in the top right of each box shows variance reduction of the corresponding component. Numbers under the station codes indicate the: epicentral distance (km) and azimuth (degree), respectively. (For interpretation of the references to colour in this figure legend, the reader is referred to the web version of this article.)

the grid search was below epicenter at depths from 2.5 to 41.5 km. As a result of this first stage of data processing we obtain a thrust mechanism whose parameters are listed in Table 3. The best-fitting mechanism is well constrained, with the condition number as low as  $CN = 2.1$ . The depth grid search is quite stable as regards to the

moment magnitude  $M_w = 3.6$ . The depth is poorly resolved, with formally best fitting solution at 8.5 km, but well acceptable depths are in the range from 5.5 to ~30 km, i.e. including the hypocenter depth (21 km). Comparing with the first-motion polarities, we observe that the best-fitting (thrust) solution of ISOLA (depth

**Table 3**  
Focal mechanism of the studied events. The (\*) indicates possible fault plane, discussed in the text.

Event	Method	Centroid depth (km)	Strike/Dip/Rake	$M_w$	VR	DC (%)
1	ISOLA	8.5	141°/37°/81° 332°/53°/97°	3.6	0.59	26
	CSPS	5.5–10.5	97°/67°/–11° 191°/80°/–157° (*)	3.5–3.6	0.56	100
2	ISOLA	25	191°/31°/170° (*) 289°/85°/59°	3.7	0.40	96
	CSPS	15–23	197°/28°/178° 289°/89°/62°	3.3–3.7	0.33	100

8.5 km) disagrees with 4 polarities: BARD, NIEB, PENA and MAUL. In this sense standard ISOLA does not provide a solution compatible with polarities. However, note that at shallow depth (5.5 km), close

to the best-fitting thrust mechanism, a strike-slip mechanism also appears in the standard ISOLA solution, and its waveform fit is almost as good as that of the thrust. Below we see that just this

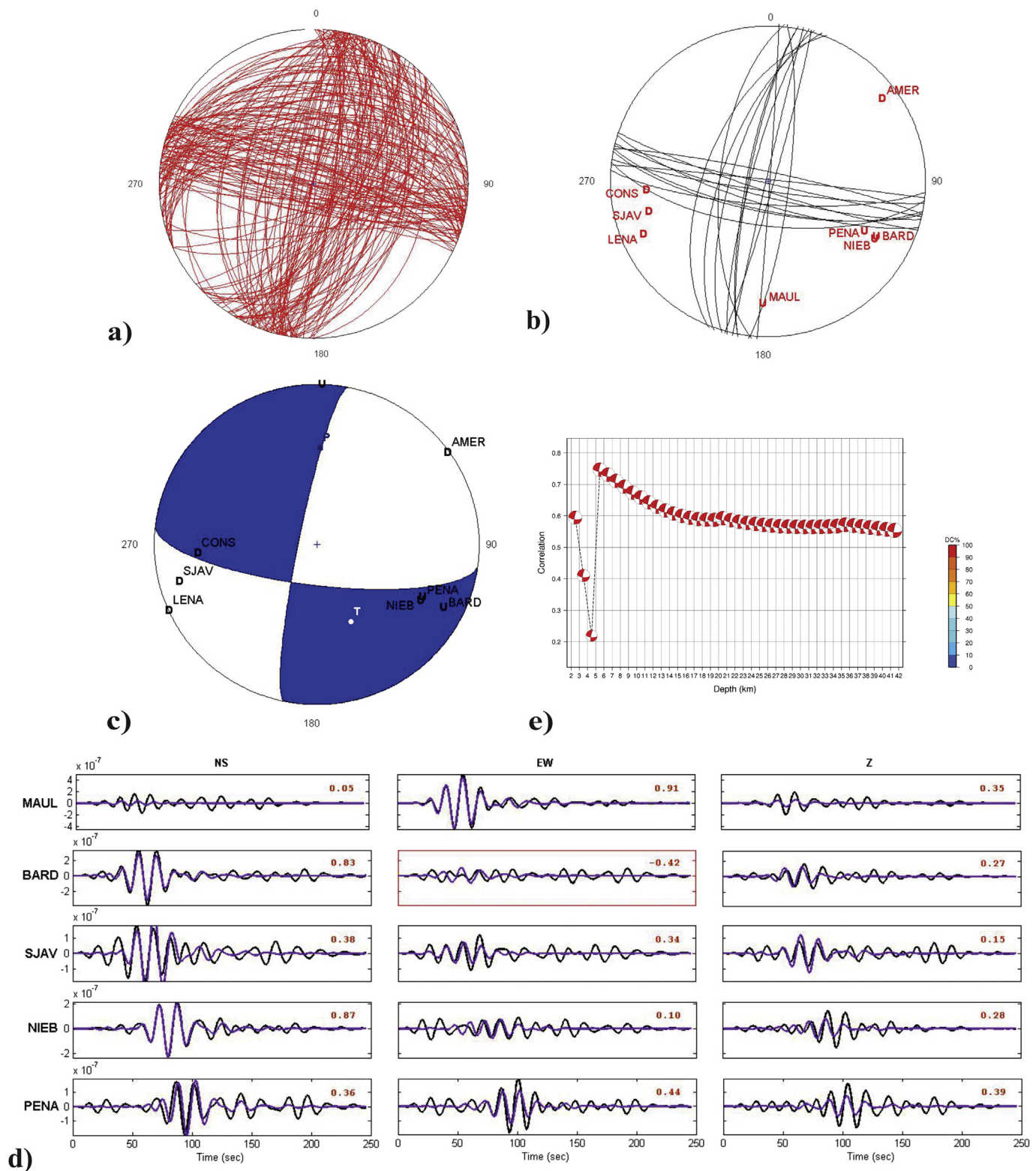


**Fig. 5.** Event 1 a) Solutions found with FOCMEC for source depth 18 km; b) Admissible solutions found with the CSPS method, ranging between 0.90  $V_{Ropt}$  and  $V_{Ropt} = 0.56$ ; c) Beachball representing the optimal solution found with the CSPS method at 5.5 km; d) Correlation diagram demonstrating variation of the waveform match with the trial source depth, using the optimal mechanism; e) Observed (black) and synthetic (purple) seismograms graphic fit. (For interpretation of the references to colour in this figure legend, the reader is referred to the web version of this article.)

solution is preferable when jointly inverting polarities and waveforms by CSPS method.

### 5.1.2. Inversion with CSPS

Using 8 polarities from stations AMER, MAUL, PENA, NIEB, BARD, CONS, SJAV and LENA, we calculate all possible first-motion polarity solutions with FOCMEC, allowing no polarity misfit. Logically, in FOCMEC we should use the hypocenter depth (21 km). However, the source depth used to project polarities on the focal sphere needs a careful consideration of the inner crustal discontinuities existing in the velocity model. For example, for the source depth of 21 km, the takeoff angle of almost all used stations is  $> 90^\circ$ , corresponding to upgoing rays; this is the effect of the 20-km discontinuity. Decreasing the assumed source depth just slightly below 20 km (e.g. 19 or 18 km), the polarity projections on focal sphere are more realistic due to waves refracted at the inner-crustal discontinuities (downgoing rays). Therefore, taking into account possible inaccuracies of the location and velocity model, we adopt the latter approach (assuming the source depth of 18 km to generate FOCMEC solutions).

The resulting focal mechanisms calculated with FOCMEC have a significant uncertainty (Fig. 5a). The plot includes diverse solutions; therefore it is important to check which of them agree with waveforms. The latter can be made by the CSPS method. We employ the same five stations as in the application of standard ISOLA in the Section 5.1.1. The frequency range and the trial source depths are also the same as in the previous section.

We apply the CSPS method and set up a range of admissible CSPS solutions in the interval between 0.90  $V_{Ropt}$  and  $V_{Ropt}$  and find 11 solutions with  $V_{Ropt} = 0.56$  (see Fig. 5b and Table 3). In this case, we do not find the thrust mechanisms, as obtained with standard ISOLA, but the solution has a strike-slip mechanism at shallow depth. The most important progress after application of

CSPS is that now the focal mechanism is in accordance with all polarities (Fig. 5c and d). The moment magnitude is quite stable over the 11 admissible solutions ( $M_w$  3.5–3.6). The depth of these solutions varies from 5.5 km (the best-fitting depth) to 10.5 km.

## 5.2. Event 2

This event occurred on 16th February 2002, see Table 2. Although, according to NEIC, its magnitude ( $M_d = 4.2$ ) is even slightly larger than the magnitude of Event 1 ( $M_d = 4.0$ ), the waveform inversion of Event 2 was feasible only for the nearest station (LENA). The likely reason why the other stations could not be fit is a larger noise compared to Event 1, and/or the larger source depth. We return to this problem in the Discussion and Conclusion section.

### 5.2.1. Inversion with ISOLA

The application of the standard ISOLA method with the single station LENA is shown in Fig. 6. The depth grid search is between 9 and 28 km. The frequency range is between 0.06 and 0.1 Hz (Fig. 6c). The obtained result is a thrust focal mechanism with a strike-slip component (see Table 3). The depth resolution is poor, but the hypocenter depth (18 km) is acceptable. However, the condition number is very large  $CN = 96$ . It is because we have just one station, representing a weakly constrained (ill-posed) problem. Thus the calculated mechanism has a very limited physical meaning unless confirmed by independent data. The first-motion polarities belong to such data, and, perhaps surprisingly, we find that the nodal planes are in agreement with the polarities projected on focal sphere for the 18 km depth (Fig. 6b). The moment magnitude is  $M_w = 3.7$ , i.e. considerably lower than by NEIC ( $M_d = 4.2$ ). To make the solution more reliable, we add the polarities into joint inversion, using the CSPS method.

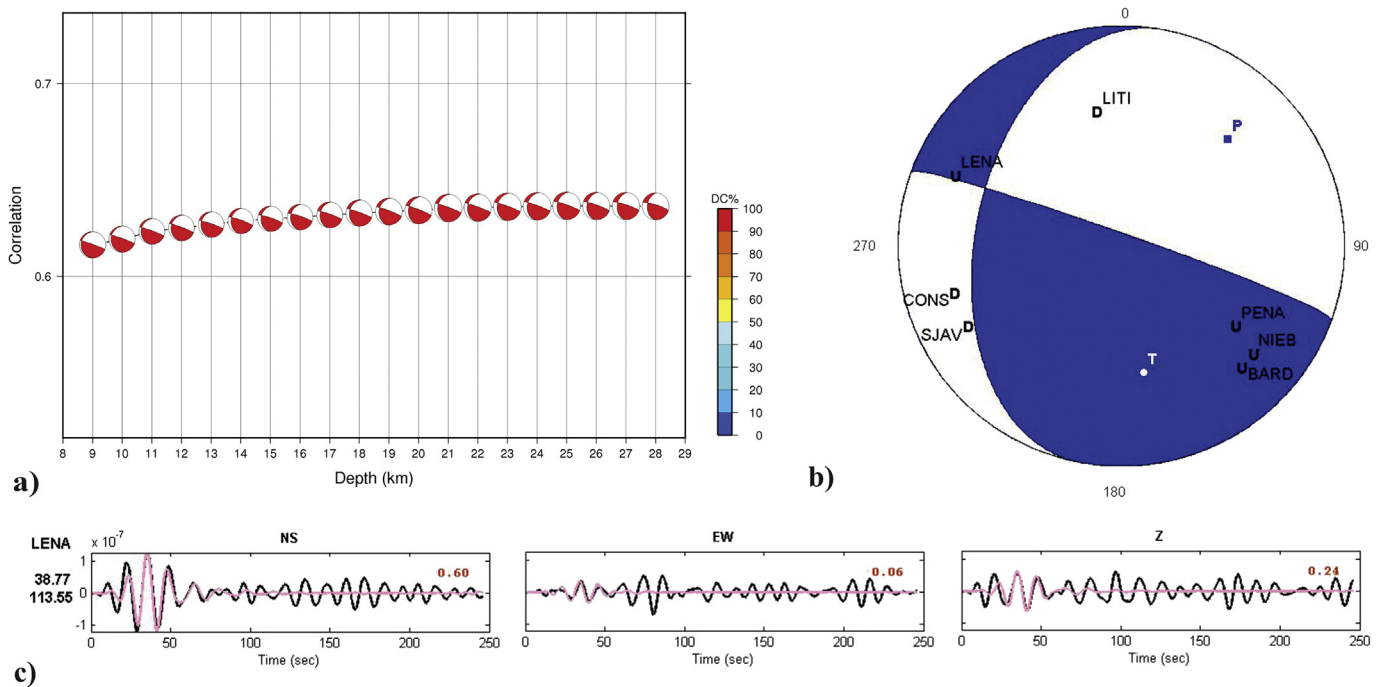


**Fig. 6.** Event 2 a) Correlation diagram demonstrating variation of the focal mechanism with the trial source depth; b) The beachball representing the optimal solution calculated by ISOLA, compared with the observed first-motion polarities for the 18 km depth; c) Observed (black) and synthetic (pink) waveforms in the frequency range between 0.06 and 0.1 Hz. Shown in the plot are displacements (in meters). The number in the top right corner of each box shows variance reduction of the corresponding component. Numbers under the station codes (left) indicate the: epicentral distance (km) and azimuth (degree), respectively. (For interpretation of the references to colour in this figure legend, the reader is referred to the web version of this article.)



### 5.2.2. Inversion with CSPS

The focal mechanisms were calculated in FOCMEC with 6 stations (PENA, NIEB, BARD, CONS, SJAV and LENA). Assuming the source depth of 18 km, we get a suite of very variable solutions; see Fig. 7a. Then the CSPS method was applied with LENA station, using similar computational parameters as in Section 5.2.1. Choosing the admissible interval between 0.50  $V_{Ropt}$  and  $V_{Ropt} = 0.33$  (Fig. 7b), intentionally broader than for Event 1 (because we have just one station with inverted waveforms) we find 3 solutions. In this case the best CSPS solution is practically the same as the standard ISOLA solution (Table 3). We can say that all admissible solutions cluster near the best solution. However, the moment magnitude range obtained by CSPS is relatively broad (3.3–3.7), and the depth range is between 15 and 23 km.

### 5.3. Discussion

The existing knowledge of the focal mechanisms of shallow weak ( $M_w < 5$ ) events in the studied region, Cordillera Principal of Argentina between  $-35^\circ$  and  $-35.5^\circ$  latitude, has been so far very limited; just six solutions have been published. Therefore, the aim of the present paper was to calculate at least a few more mechanisms by waveform inversion, making use of broad-band data from the recent temporary seismic experiment CHARGE. Preliminary tests and an intensive search for usable data resulted in 2 events (Table 2). Their focal mechanisms, included in Fig. 8, were studied

in detail using two methods, ISOLA and CSPS.

Different techniques had used to obtain the principal stress orientations from a population of focal mechanisms or from the original data of polarities and take-off angles used to calculate them (Harmsen and Rogers, 1986; Rivera and Cisternas, 1990; Reyners et al., 2002). In the region under study, considering the few focal mechanisms available, we cannot make assumptions about the stress pattern. However we suggest some hypotheses (which are not the unique) to explain the focal mechanisms obtained in this work. A rigorous tectonic regime can be assigned when more earthquake focal mechanisms from local or regional studies become available.

The Event 1 present two solutions, strike-slip mechanism with a normal component (Fig. 5 c) and thrust mechanism (Fig. 4b). The more robust solution is the strike-slip solution considering it is in agreement with polarities. The CSPS method has shown that the two nodal planes are well constrained (Fig. 5b). The moment magnitude of this event is well resolved ( $M_w = 3.6$ ), and it is lower than the NEIC estimation ( $M_d = 4.0$ ), but bear in mind the difference between the methods of calculating both magnitudes. In contrast to the hypocenter location (21 km), the CSPS method suggests a very shallow depth (5.5 and 8.5 km). This disagreement may be caused by the relatively large epicentral distances of the stations used. To locate reliably a shallow event like this by means of first arrival times we would need P and S readings from stations at epicentral distances of the order of  $\sim 10$  km, or less, and a very

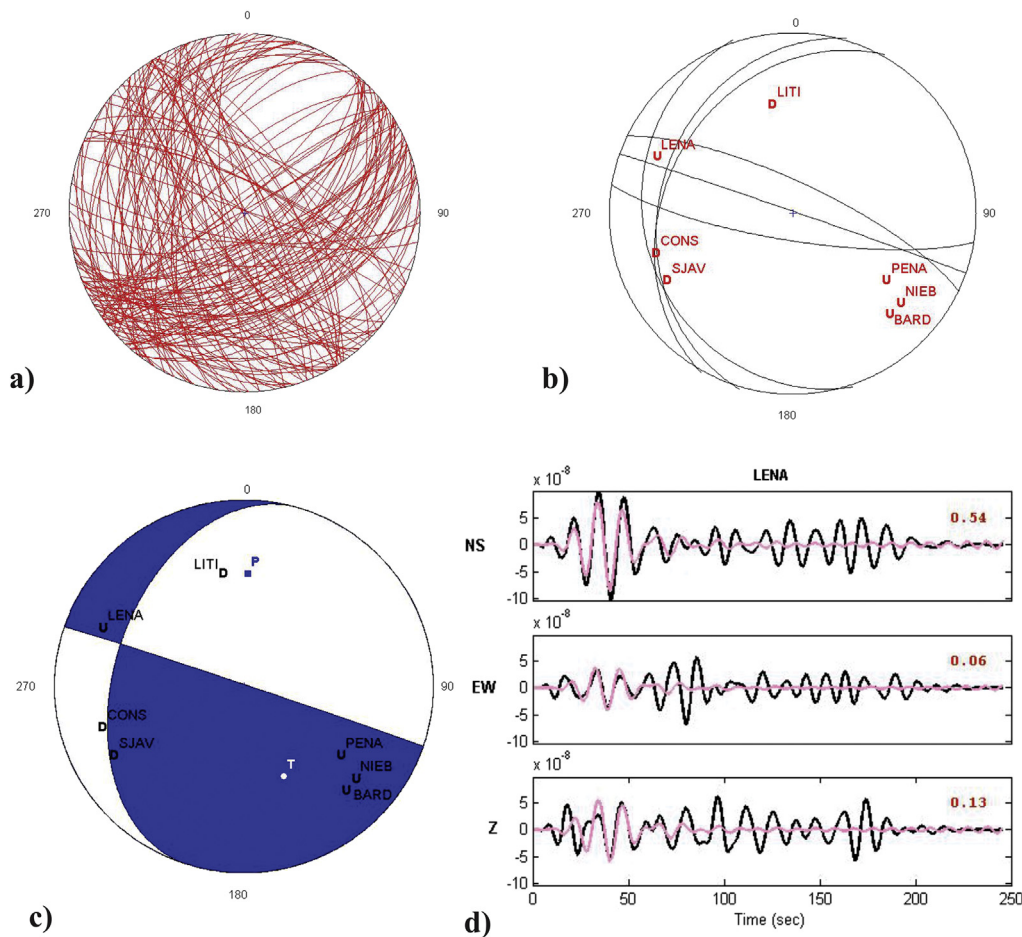


**Fig. 7.** Event 2 a) Solutions found with FOCMEC for the source depth of 18 km; b) Admissible solutions found with the CSPS method, ranging between 0.50  $V_{Ropt}$  and  $V_{Ropt} = 0.33$ ; c) Beachball representing the optimal solution found with the CSPS method, polarities plotted for the depth of 18 km; d) Observed (black) and synthetic (pink) seismograms graphic fit. (For interpretation of the references to colour in this figure legend, the reader is referred to the web version of this article.)



detailed velocity model of the uppermost crustal layers. The waveform inversion at the available stations (epicentral distances between 71 and 213 km) is more sensitive to the shallow depth because the records contain also surface waves. This issue has to be studied in more detail elsewhere, similarly to the disagreement between hypocenter and centroid depth found by Zahradník et al. (2008) and Janský et al. (2009), but the obtained indication of a very shallow depth is rather strong. The thrust mechanism of Event 1 and the centroid depth similar to the hypocenter depth cannot be ruled out, but with the existing velocity model such a solution seems less likely due to a few polarity disagreements.

From a geological analysis, this earthquake (Event 1) is located at the western part of the Malargüe Fault and Thrust belt. This is a typical thick skinned structural style related to the partially inverted Mesozoic deposits to the Neuquén basin (Giambiagi et al., 2009). The focal mechanism of this earthquake could be related to the movement of the Calabozos fault system described at field studies by Tapia (2010). This fault was described like a reverse fault dipping 20 to 30°W up to 60°W and oriented N–S up to NNW–SSE. Particularly, this sector not has geophysical studies related to the microearthquakes but, one of the field observations of Tapia (2010) were that this fault cut the glacial and post-glacial sequence concluded has quaternary activity. According with Farías et al. (2010) the current state of the Cordillera Principal would have a

kinematic predominantly dextral with a forearc advancing north, that is consistent with a dextral strike slip component and nodal plane located in N–S direction. The reverse component is better explained by the Calabozos fault.

The analysis of Event 2 is more difficult, because the waveforms could be successfully modeled only with a single (nearest) station. As such, with just a single station, the standard waveform inversion with ISOLA is very poorly constrained. Nevertheless, in this particular case the ISOLA solution luckily satisfies the first-motion polarities, thus the best CSPA solution and ISOLA solution are the same. The mechanism is a thrust with a strike-slip component. The CSPA method provides an uncertainty estimate, showing that the admissible solutions form a relatively compact cluster around the best-fitting solution. The centroid depth is poorly constrained, but the hypocenter depth (18 km) is not ruled out. The moment magnitude ( $M_w \sim 3.3\text{--}3.7$ ) is also poorly constrained, although definitely lower than the  $M_d = 4.2$  of NEIC.

Event 2 could be related to the El Diablo–El Fierro fault system. This fault corresponds to the eastern border of the Abanico basin (Charrier et al., 2002). The plane of the fault is oriented N–S to NNE–SSW dipping west and correspond to the tectonic contact between Cenozoic and Mesozoic sequences. This fault has a normal movement at Mesozoic and Eocene–Oligocene times and was partially inverted at the Miocene. These compressive movements

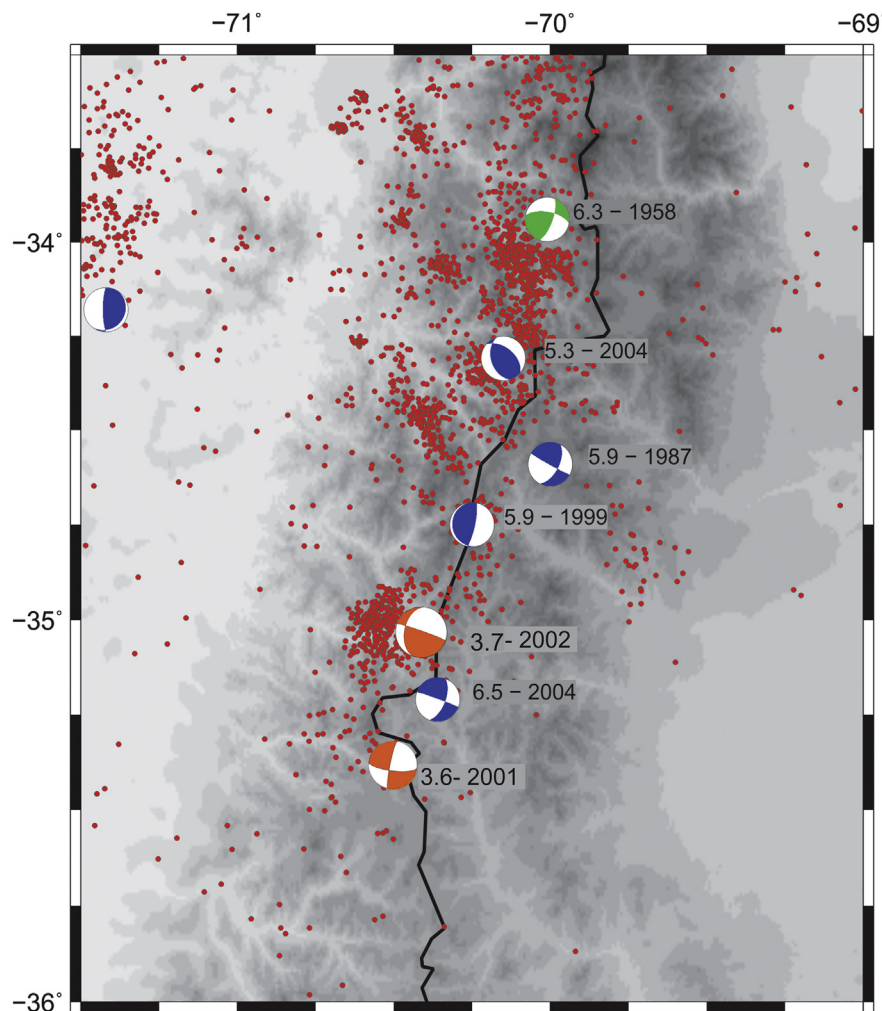


**Fig. 8.** Same as in Fig. 2, but including the two mechanisms calculated in the present paper (in orange). (For interpretation of the references to colour in this figure legend, the reader is referred to the web version of this article.)

correspond to the tectonic inversion of the Abanico Basin (Charrier et al., 2002).

The El Diablo–El Fierro fault system has several microearthquakes along this fault recognized by many authors (Comte et al., 2008; Farías et al., 2008). The associated seismic activity implies that this structure is still active and participates in the present-day adjustments of the Andean crust. The shallow earthquake of  $M_w = 6.5$  of August 28th, 2004, was studied by Comte et al. (2008), and had the solution similar to the event 2 analyzed in this work. Both are possibly associated with the El Diablo–El Fierro fault system have strike-slip displacements and N–S or NNE–SSW oriented vertical planes. The only difference in this comparison is the event 2 has a subhorizontal plane. This could be related to the detachment level at depth of this fault system like was proposed by Charrier et al. (2002), Farías et al. (2010), y Piquer et al. (2010) at these latitudes. According with Farías (2007) the current state of the Main Cordillera would have a kinematic predominantly dextral course with a forearc toward advancing to the north.

Dextral strike-slip solutions strike-slip dextral are consistent with recent studies in the area, which show that the region had evidence of these structures (Tapia et al. 2015), which were reactivated by the earthquake of February 27, 2010, Maule, Chile (Lupi and Miller, 2014; and Spagnotto et al., 2015).

Although two mechanisms were added to the previously existing six mechanisms, future investigation in the region should considerably increase the number of reliably inverted events, optimally with temporary local networks.

## 6. Conclusion

In this work focal mechanisms of two crustal seismic events in the Andean chain were obtained. The southernmost event (Event 1) has a strike-slip solution with a normal component. We proposed that its north-south nodal plane with right lateral displacement could be associated with Calabozos fault system. The magnitude  $M_w$  3.6 achieved for this event is lower than the magnitude provided by NEIC ( $M_d = 4.0$ ). Also the depth obtained from waveforms (5.5–5.8 km) is considerably smaller than the hypocenter location depth (21 km). For the northernmost event (Event 2), characterized by a strike-slip solution with a small thrust component, we suggested an interpretation in terms of an activation of a detachment level of the El Diablo–El Fierro thrust fault system. The magnitude is poorly constrained (3.3–3.7), but definitely lower than that of NEIC ( $M_d = 4.2$ ). The depth for this event from the waveform inversion methods varies in a broad range, so in this case our preferred hypocenter location depth is 18 km. Such depth is also related with our interpretation of the activated detachment level and with subhorizontal nodal plane being the fault plane.

The difference between the obtained magnitudes and NEIC magnitudes is understandable considering that NEIC reports duration magnitude. Future studies are needed to establish scaling relations between various magnitudes of small events ( $M_d$ ,  $M_L$ ,  $M_w$ ) in the studied region.

## Acknowledgments

The facilities of the IRIS Data Management System, and specifically the IRIS Data Management Center, were used for access to waveform, metadata or products required in this study. The IRIS DMS is funded through the National Science Foundation and specifically the GEO Directorate through the Instrumentation and Facilities Program of the National Science Foundation under Cooperative Agreement EAR-0552316. Some activities of are supported by the National Science Foundation EarthScope Program under Cooperative Agreement EAR-0733069. One of the authors

(J.Z.) has been supported from the Czech Science Foundation grant GACR-14-04372S. The authors wish to thank to Efthimios Sokos and Lucia Fojtíková for valuable help during this work.

## References

- Alvarado, P., 1998. Sismicidad superficial de los Andes Centrales (33°–35°S; 69.5°–70.5°W). Departamento. Geofísica, Universidad de Chile, p. 161. Tesis de Magister en Ciencias, mención Geofísica.
- Alvarado, P., Barrientos, S., Sáez, M., Astroza, M., Beck, S., 2009. Source study and tectonic implications of the historic 1958 Las Melosas crustal earthquake, Chile, compared to earthquake damage. *Phys. Earth Planet. Interiors* 175, 26–36. <http://dx.doi.org/10.1016/j.pepi.2008.03.015>.
- Anderson, M.L., Alvarado, P., Zandt, G., Beck, S., 2007. Geometry and brittle deformation of the subducting Nazca Plate Central Chile and Argentina. *Geophys. J. Int.* 171, 419–434.
- Barrientos, S., Vera, E., Alvarado, P., Monfret, T., 2004. Crustal seismicity in central Chile. *J. S. Am. Earth Sci.* 16, 759–768.
- Beck, S., Barrientos, S., Kausel, E., Reyes, M., 1998. Source characteristics of historic earthquakes along the central Chile subduction zone. *J. S. Am. Earth Sci.* 11, 115–129.
- Bouchon, M., 1981. A simple method to calculate Green's functions for elastic layered media. *Bull. Seismol. Soc. Am.* 71, 959–971.
- Charrier, R., Baeza, O., Elgueta, S., Flynn, J.J., Gans, P., Kay, S.M., Muñoz, N., Wyss, A.R., Zurita, E., 2002. Evidence for Cenozoic extensional basin development and tectonic inversion south of the flat-slab segment, southern Central Andes, Chile (33°–36°S.L.). *J. S. Am. Earth Sci.* 15, 117–139.
- Christensen, D.H., Ruff, L.J., 1988. Seismic coupling and outer rise earthquakes. *J. Geophys. Res.* 93, 13, 421–513, 444.
- Comte, D., Farías, M., Charrier, R., González, A., 2008. Active tectonics in the central Chilean Andes; 3D tomography based on the aftershock sequence of the 28 August 2004 shallow crustal earthquake Abstracts with Programs AGU Fall Meeting, Eos, Transactions, 89 (53, Suppl.): T41A–193.
- Farías, M., 2007. Tectonique, erosion et evolution du relief dans les Andes du Chile Central au cours du neogene. Université Toulouse III, Santiago de Chile, p. 238. Ph.D. Thesis.
- Farías, M., Charrier, R., Carretier, S., Martinod, J., Fock, A., Campbell, D., Cáceres, J., Comte, D., 2008. Late Miocene high and rapid surface uplift and its erosional response in the Andes of Central Chile (33°–35°S). *Tectonics* 27, TC1005.
- Farías, M., Comte, D., Charrier, R., Martinod, J., Claire, D., Tassara, A., Tapia, F., Fock, A., 2010. Crustal-scale structural architecture in Central Chile based on seismicity and surface geology: implications for Andean mountain building. *Tectonics* 29. <http://dx.doi.org/10.1029/2009TC002480>. TC3006.
- Fojtíková, L., Zahradník, J., 2014. A new strategy for weak events in sparse networks: the first-motion polarity solutions constrained by single-station waveform inversion. *Seismol. Res. Lett.* 85, 1265–1274. <http://dx.doi.org/10.1785/0220140072>.
- Giambiagi, L., Ghiglione, M., Cristallini, E., Bottesi, G., 2009. Características estructurales del sector sur de la faja plegada y corrida de Malargüe (35°–36°S): distribución del acortamiento e influencia de estructuras previas. *Rev. Asoc. Geol. Argent.* 65, 140–153.
- Harmsen, S.C., Rogers, A.M., 1986. Inferences about the local stress field from focal mechanisms: applications to earthquakes in the southern Great Basin of Nevada. *Bull. Seismol. Soc. Am.* 76, 1560–1572.
- Havskov, J., Ottemöller, L., Canabrava, R.L.P., 2007. SEISAN: multiplatform implementation of MINISEED/SEED. *Orfeus Newsl.* 7 (2).
- Janský, J., Zahradník, J., Plicka, V., 2009. Shallow earthquakes: shallower than expected? *Studia Geophys. Geod.* 53, 261–268.
- Kendrick, E., Bevis, M., Smalley, R.J., Brooks, B.A., Barriga, R., Lauría, E., Souto, L.P., 2003. The Nazca–South America Euler vector and its rate of change. *J. S. Am. Earth Sci.* 16, 125–131.
- Křížová, D., Zahradník, J., Kíratzi, A., 2013. Resolvability of isotropic component in regional seismic moment tensor inversion. *Bull. Seismol. Soc. Am.* 103, 2460–2473. <http://dx.doi.org/10.1785/0120120097>.
- Lange, D., Tilmann, F., Barrientos, S.E., Contreras-Reyes, E., Methe, P., Moreno, M., Heit, B., Agurto, H., Bernard, P., Vilotte, J.P., Beck, S., 2012. Aftershock seismicity of the 27 February 2010  $M_w$  8.8 Maule earthquake rupture zone. *Earth Planet. Sci. Lett.* 317–318, 413–425.
- Lavenue, A., Cembrano, J., 1999. Compressional and transpressional stress pattern for the Pliocene and Quaternary (Andes of central and southern Chile). *J. Struct. Geol.* 21, 1669–1691.
- Lay, T., 2015. The surge of great earthquakes from 2004 to 2014. *Earth Planet. Sci. Lett.* 409, 133–146.
- Lienert, B., Havskov, J., 1995. A computer program for locating earthquakes locally, regionally and globally. *Seismol. Res. Lett.* 66, 26–36.
- Lupi, M., Miller, S.A., 2014. Short-lived tectonic switch mechanism for long-term pulses of volcanic activity after mega-thrust earthquakes. *Solid Earth* 5, 13–24. <http://dx.doi.org/10.5194/se-5-13-2014>.
- Marot, M., 2013. Flat versus Normal Subduction Zones: a Comparison Based on 3-D Regional Travel-time Tomography and Petrological Modeling of Central Chile and Western Argentina (29°–35°S). Ph.D. Thesis. Université de Nice-Sophia Antipolis - UFR Sciences, France, p. 224 (in English).
- Moreno, M.S., Bolte, J., Klotz, J., Melnick, D., 2009. Impact of megathrust geometry

- on inversion of coseismic slip from geodetic data: application to the 1960 Chile earthquake. *Geophys. Res. Lett.* L16310 (36). <http://dx.doi.org/10.1029/2009GL039276>.
- Nacif, S., 2012. Seismotectonic of the Nazca Plate between 33°S and 35°S below the Interplate Seismogenic Zone and Seismic Anisotropy in the Crust and the Upper Mantle of the Overriding Plate. Ph.D. Thesis. San Juan University, Argentina, p. 217 (in Spanish).
- Pardo, M., Comte, D., Monfret, T., 2002. Seismotectonic and stress distribution in the central Chile subduction zone. *J. S. Am. Earth Sci.* 15, 11–22.
- Piquer, J., Castelli, J.C., Charrier, R., Yáñez, G., 2010. El Cenoico del alto río Teno, Cordillera Principal, Chile central: estratigrafía, plutonismo y su relación con estructuras profundas. *Andean Geol.* 37 (1), 32–53.
- Reyners, M., Robinson, R., Pancha, A., McGinty, P., 2002. Stresses and strains in a twisted subduction zone - Fiordland, New Zealand. *Geophys. J. Int.* 148, 637–648.
- Rivera, L., Cisternas, A., 1990. Stress tensor and fault plane solutions for population of earthquakes. *Bull. Seismol. Soc. Am.* 80 (3), 600–614.
- Ruiz, S., Grandin, R., Dionicio, V., Satriano, C., Fuenzalida, A., Vignyc, C., Kiraly, E., Meyer, C., Baez, J.C., Riquelme, S., Madariaga, R., Campos, J., 2013. The Constitución earthquake of 25 March 2012: a large aftershock of the Maule earthquake near the bottom of the seismogenic zone. *Earth Planet. Sci. Lett.* 377–378, 347–357.
- Snoke, J.A., 2003. In: Lee, W.H.K., Kanamori, H., Jennings, P.C., Kisslinger, C. (Eds.), *FOCMEC: FOCal MECHANism Determinations, International Handbook of Earthquake and Engineering Seismology*. Academic Press, San Diego, pp. 1629–1630. Chapter 85.12.
- Sokos, E., Zahradník, J., 2008. ISOLA a FORTRAN code and a Matlab GUI to perform multiple-point source inversion of seismic data. *Comput. Geosci.* 34, 967–977.
- Sokos, E., Zahradník, J., 2013. Evaluating Centroid-moment-tensor Uncertainty in the New Version of ISOLA Software.
- Spagnotto, S., 2013. Sismicidad entre 34.5°-36.5°S y 67°-71°O posterior al sismo de Maule, Mw=8.8, 27/02/2010 y distribuciones de deslizamientos en placa de Nazca para sismos de profundidades mayores a 100 km en secciones plana y normal entre 31-34°S. Universidad Nacional de San Juan, Facultad de Ciencias Exactas, Físicas y Naturales, Instituto Geofísico Sismológico Volponi. Ph.D. Thesis.
- Spagnotto, S., Triep, E., Giambiagi, L., Lupari, M., 2015. Triggered seismicity in the Andean arc region via static stress variation by the Mw=8.8, February 27, 2010, Maule earthquake. *J. S. Am. Earth Sci.* 63, 36–47.
- Tapia, F., 2010. Análisis estructural del sector occidental de la Faja Plegada y Corrida de Malargüe en el curso superior del río Colorado de Lontué (35°18'-35°23'), Región del Maule, Chile, p. 134. Tesis de licenciatura. Universidad de Chile. Inédita.
- Tapia, F., Farías, M., Naipauer, J., 2015. Late cenozoic contractional evolution of the current arc-volcanic region along the southern Central Andes (35°20S). *J. Geodyn.* 88, 36–51.
- Zahradník, J., Janský, J., Plicka, V., 2008. Detailed waveform inversion for moment tensors of M=4 events; examples from the Corinth Gulf, Greece. *Bull. Seismol. Soc. Am.* 98, 2756–2771.
- Zahradník, J., Custódio, S., 2012. Moment tensor resolvability: application to southwest Iberia. *Bull. Seismol. Soc. Am.* 102, 1235–1254. <http://dx.doi.org/10.1785/0120110216>.